Supplementary Information for

Observed thresholds in sea-level rise driving global tidal wetland loss

Jiejun Luo[1,2], Avril Hardi[2], Zhijun Dai[1]*, Wiebe Nijland[2], Xuefei Mei[1], Jie Wang[1,3], Jaap H. Nienhuis[2]*

[1]State Key Laboratory of Estuarine and Coastal Research, East China Normal University, Shanghai, China

[2]Department of Physical Geography, Utrecht University, Utrecht, the Netherlands

[3]State Key Laboratory of Climate Resilience for Coastal Cities, Department of Civil and Environmental Engineering, The Hong Kong Polytechnic University, Hong Kong, China

*Correspondence to: Prof. Zhijun Dai (zjdai@sklec.ecnu.edu.cn) or Dr. Jaap H. Nienhuis (j.h.nienhuis@uu.nl).

Contents

Supplementary Discussion 2
Supplementary Methods 5
Random sampling based on uncertainty intervals 5
Supplementary Figures 1–22 7
Supplementary Tables 1–5 29
References 32

Supplementary Discussion

Why don't we define thresholds for areal responses using collapse probabilities in the same way as for vertical processes?

In studies of tidal wetland responses to relative sea-level rise (RSLR), the definition of the threshold rate can strongly influence results, in addition to differences in reported values (Table 1). In recent studies, thresholds are often defined probabilistically: an ecosystem is considered to exceed its threshold when it has a certain probability (e.g., 90%) of collapse under a given RSLR rate. However, it is important to note that this probabilistic definition is closely linked to the underlying physical processes.

For vertical processes, the effects of sea-level rise are direct, primarily through inundation of low-lying areas. Changes in surface elevation, including sediment accretion and subsidence, are strongly and directly related to RSLR, with consistent physical units, allowing the relative change to be calculated directly by subtraction. This is reflected in recent studies of vertical thresholds: RSLR rate thresholds are typically computed from binary (positive/negative) or ternary (positive/stable/negative) probability distributions[1–4]. These studies show that when RSLR rate is near zero, the probability of a deficit is also close to zero (or at a low level), whereas higher RSLR rates correspond to probabilities approaching 100%. In other words, the range of observed RSLR rates in these vertical studies nearly covers all possible deficit probabilities.

In contrast, lateral processes such as contraction or loss are influenced by factors beyond elevation surplus/deficit. As a result, the probability of loss is non-zero even at

near-zero RSLR, and maximum probabilities often do not reach 100%. For example, Saintilan et al. (ref. [3]) shows that probabilities of contraction and water conversion in tidal marshes neither start from zero nor reach 100%, and our results (Fig. 2a–c) show similar patterns. This indicates that area loss cannot be fully attributed to RSLR alone. Moreover, because probabilities do not reach a predefined level (e.g., 90%), it is not straightforward to assign a corresponding RSLR threshold. Using similar probability-based definition in our area change study, we find that for salt marshes, a 66% loss probability corresponds to ~12 mm yr^{-1} RSLR, but the 90% probability cannot be determined (Fig. 2b). For mangroves, the 90% loss probability corresponds to ~13 mm yr^{-1}, but the 66% probability cannot be defined because baseline loss probabilities are already above 66% under all observed RSLR conditions (Fig. 2c). This demonstrates that applying the same RSLR threshold definition used for vertical processes does not allow a comprehensive or robust attribution of the role of sea-level rise in area loss.

Additionally, the presence of landward migration means that areal change inherently lags behind vertical elevation change[5,6]. As a result, observed signals of area loss include, but are not equivalent to, direct inundation. The corresponding threshold therefore represents the “last line of defense” for maintaining wetland shorelines rather than the onset of vertical failure. Notably, when applying the same probability-based definition used for vertical processes, the thresholds derived from our data are substantially higher (salt marshes: 66% loss at ~12 mm yr^{-1}; mangroves: 90% loss at ~13 mm yr^{-1}) than reported vertical thresholds from studies of modern vertical processes (e.g., salt marshes[2]: 90% deficit at 7.6 mm yr^{-1}; mangroves[3]: 90% deficit at

7.9 mm yr^{-1}; Table 1).

Moreover, these probability-based thresholds for area change are higher than the threshold inferred from our analysis based on the variability of net change (~9 mm yr^{-1}), indicating that reliance on this definition alone would substantially overestimate the RSLR threshold. Such overestimation may lead to overly optimistic projections of wetland persistence and delay timely, targeted management and adaptation strategies. Therefore, distinguishing between vertical and lateral definitions of RSLR thresholds is critical for future research and effective coastal wetland management.

Supplementary Methods

Random sampling based on uncertainty intervals

To propagate uncertainty in grid-cell estimates, we generated random samples for each Monte Carlo realization according to the shape of the reported uncertainty intervals:

1. **Symmetric intervals**: For grid cells with approximately symmetric uncertainty, random values were sampled from a normal distribution using the reported median ($y_{M,k}$) as the mean and the half-width of the uncertainty interval as the standard deviation.

2. **Positively skewed intervals**: For grid cells with positively skewed uncertainty intervals, gamma distributions were fitted using the median ($y_{M,k}$), lower ($y_{L,k}$), and upper ($y_{U,k}$) bounds. Sampling was then performed directly from the fitted gamma distribution.

3. **Negatively skewed intervals**: For negatively skewed intervals, a transformation was applied to convert the interval into a positively skewed form suitable for gamma sampling. Specifically, for each cell k, an expansion value was defined as:

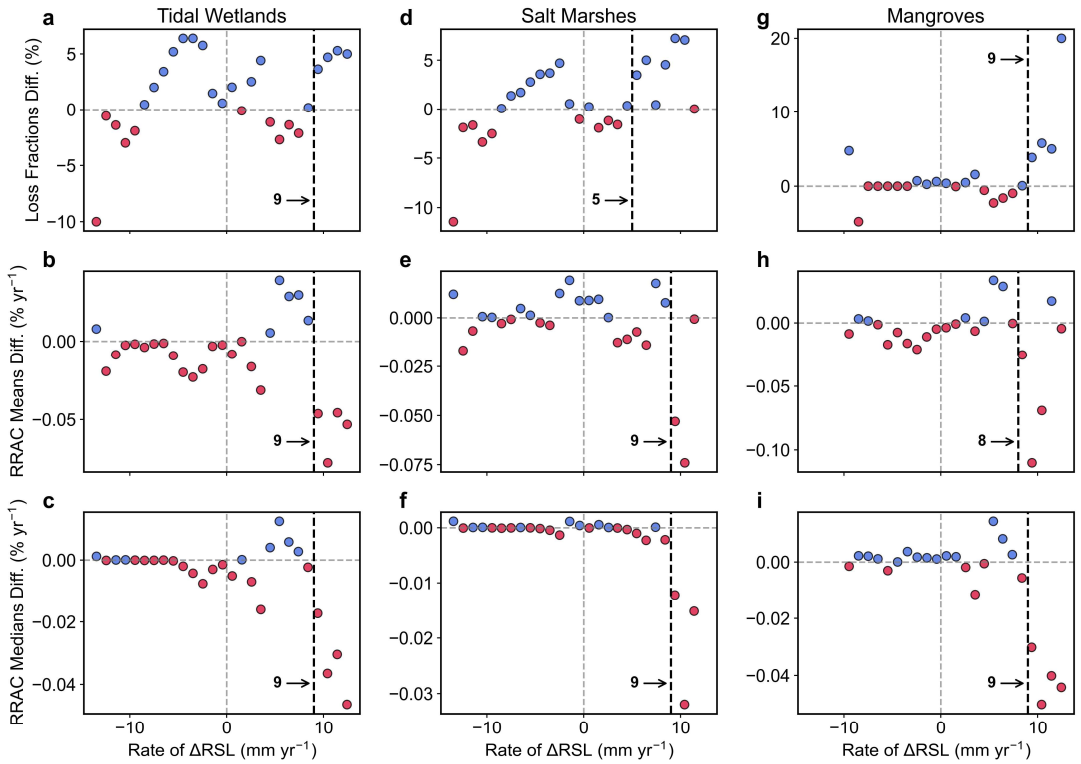
$$Y_k = y_{U,k} + 1.5 \times (y_{U,k} - y_{M,k})$$

The original median, lower, and upper bounds were subtracted from Y_k, producing a positively skewed distribution. Gamma-based sampling was then applied to this transformed distribution. After sampling, the original scale was

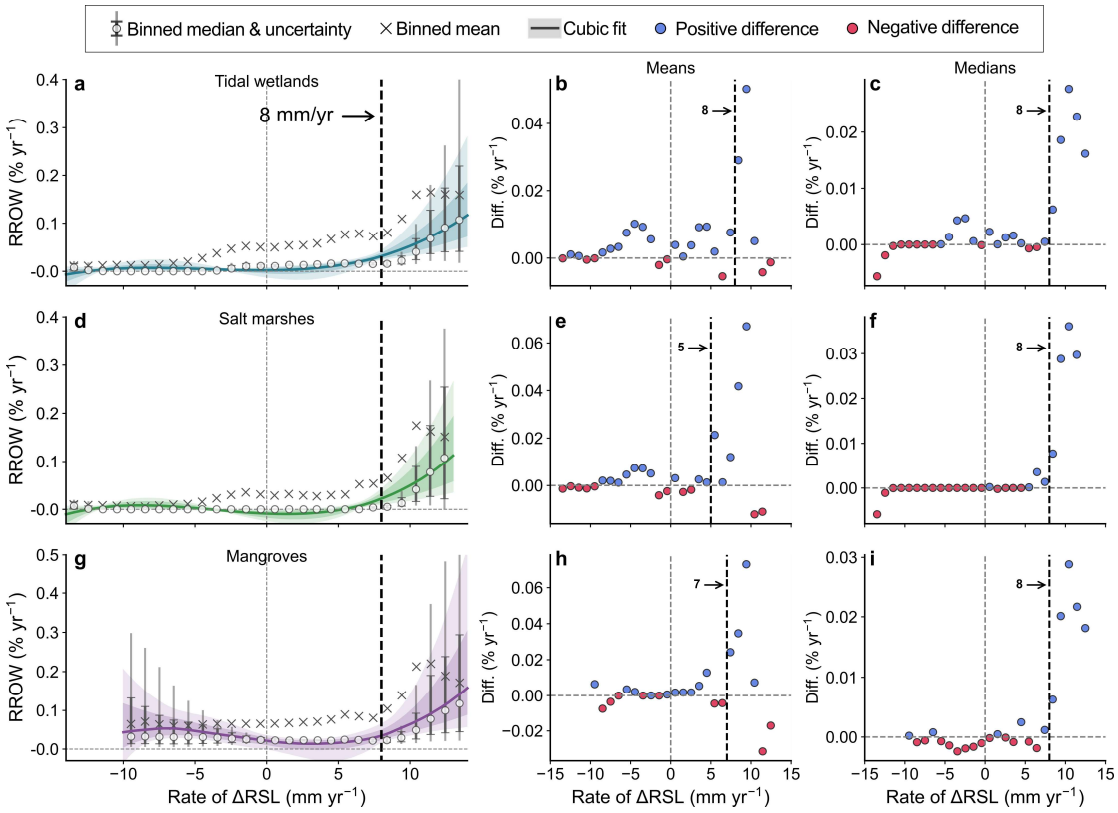
restored by subtracting the sampled values from Y_k.

4. **Evaluation of sampling reliability**: To verify the method, we compared the median and 2.5th/97.5th percentiles ($y'_{M,k}, y'_{L,k}, y'_{U,k}$) of the sampled distributions with the original input values ($y_{M,k}, y_{L,k}, y_{U,k}$) across all grid cells (Supplementary Figure 16). Deviations were minimal, confirming the reliability of this approach for representing asymmetric uncertainties.

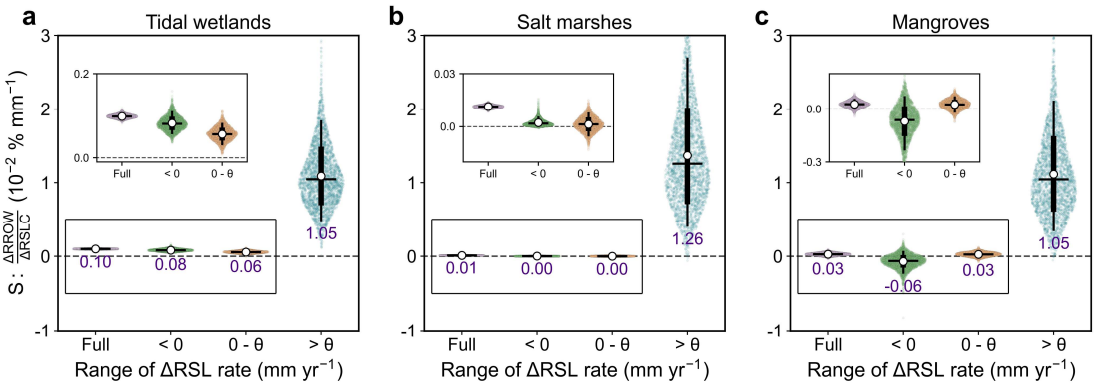
Supplementary Figures 1–22



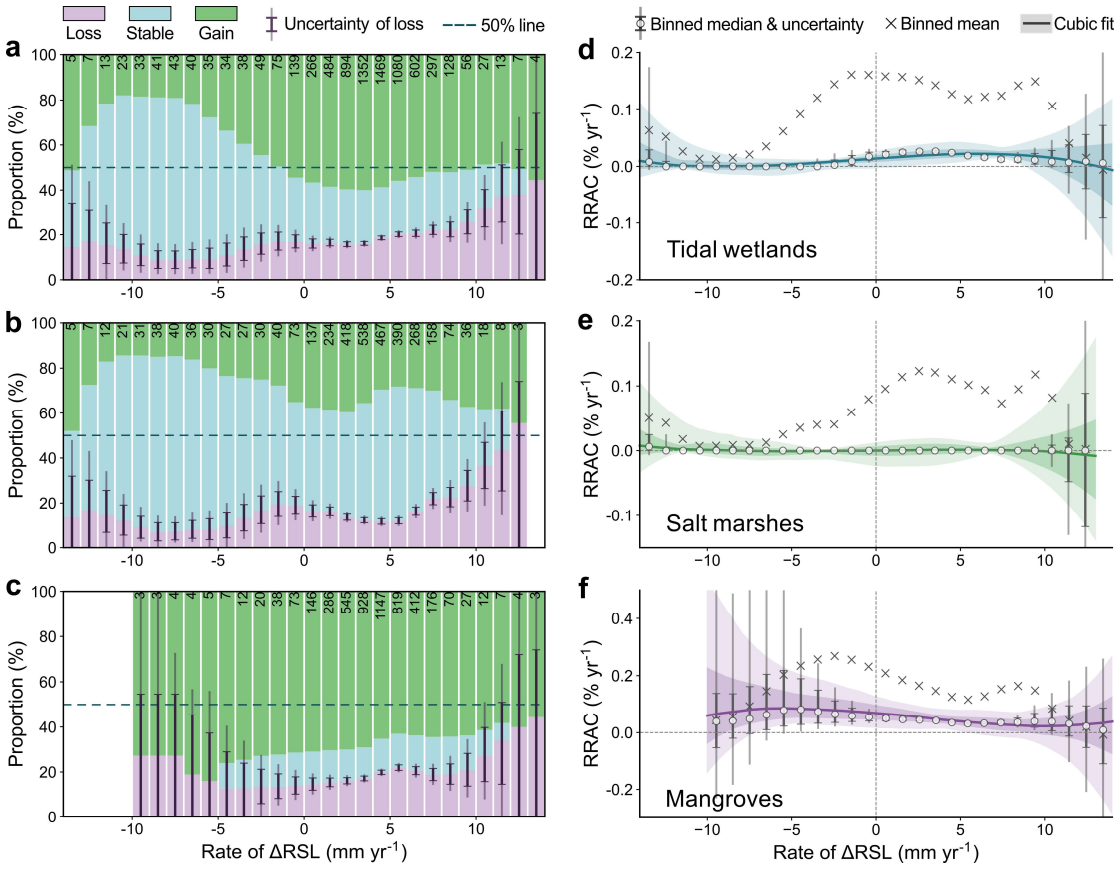
Supplementary Figure 1 | Threshold identification across different metrics. Bin-to-bin differences in loss fraction, and in mean and median relative rates of net area change across relative sea-level change rates, are shown separately for (a–c) all tidal wetlands, (d–f) salt marshes and (g–i) mangroves. Differences between each adjacent bin pair (later minus earlier) are plotted at the midpoint of the earlier bin. Red and blue circles indicate negative and positive differences, respectively. The black vertical dashed lines mark the left edges (lower boundaries) of the identified bins, indicating the onset points where each wetland type shows increased loss fraction and abrupt declines in area change rate (based on both binned means and medians). The maximum of these three threshold positions is adopted as the final critical threshold for abrupt area loss.



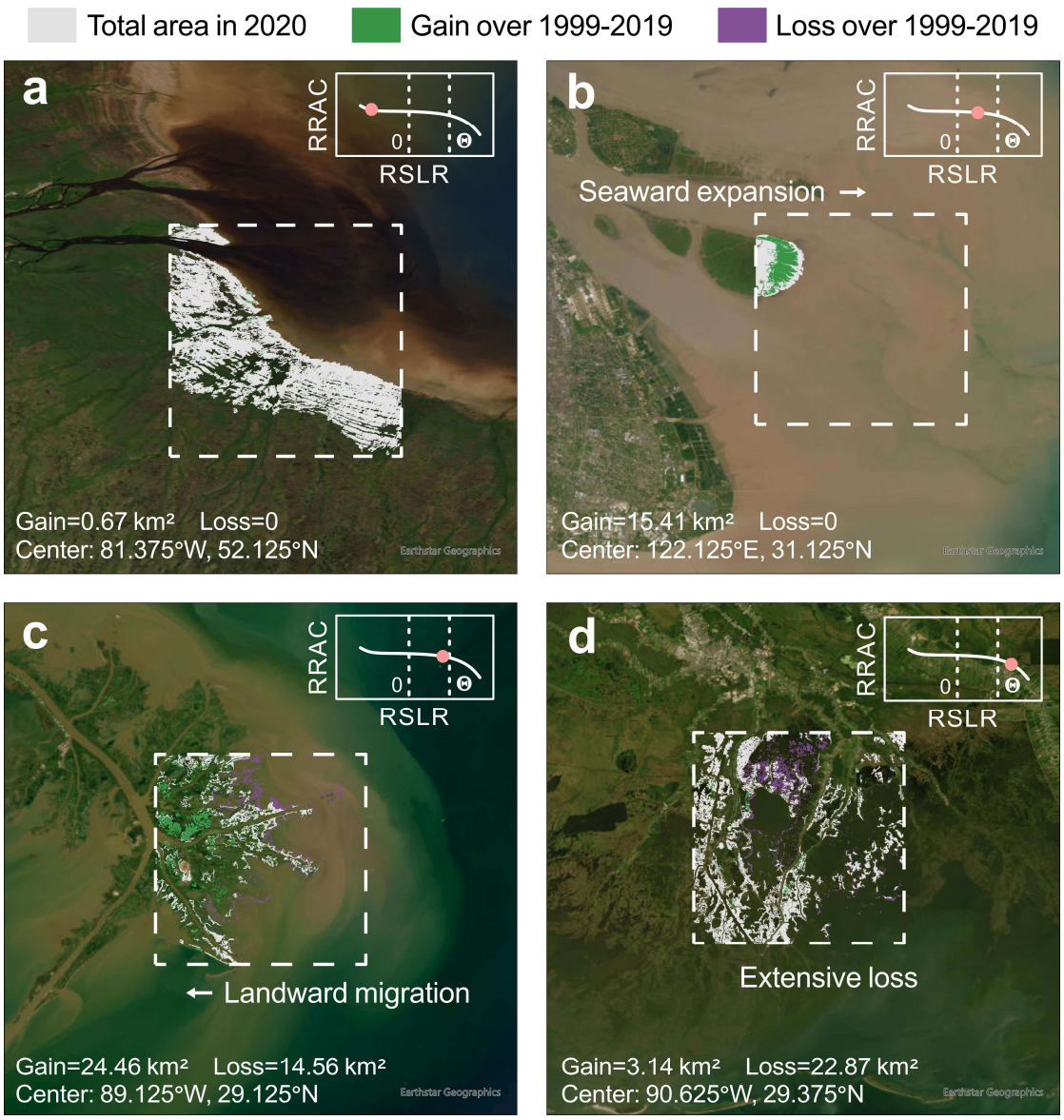
Supplementary Figure 2 | Effect of relative sea-level change on wetland conversion to open water. Trends in relative rate of conversion to open water as a function of relative sea-level change rate are shown for (a) all tidal wetlands, (d) salt marshes and (g) mangroves. Circles and crosses denote the medians of binned medians and binned means, respectively. Grey error bars represent the 66% and 90% uncertainty ranges. The black vertical dashed line marks the threshold position, taken as the maximum of the values identified in the two right-hand panels. The colored curves show cubic fit to the binned medians, with darker and lighter shaded envelopes indicating the 66% and 90% uncertainty ranges. Only bins containing more than three grid cells are shown. Correspondingly, bin-to-bin differences in means (b, e, h), and medians (c, f, i) across relative sea-level change rates are shown for tidal wetlands, salt marshes and mangroves. Red and blue circles indicate negative and positive differences, respectively. The black vertical dashed lines mark the left edges (lower-boundary) of the identified bins, representing the onset points where the same wetland type exhibits abrupt loss acceleration (as indicated by both binned means and medians).



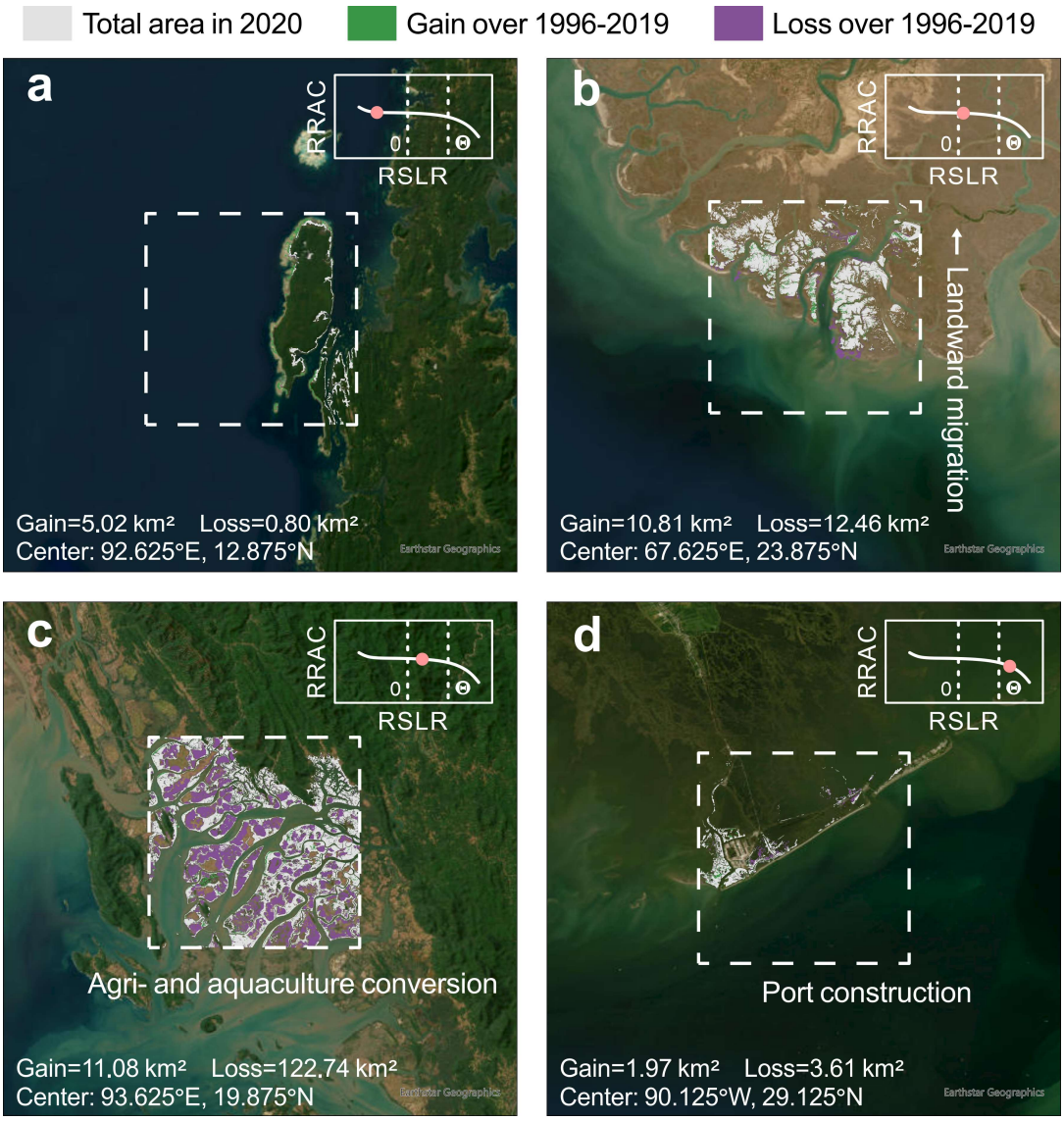
Supplementary Figure 3 | Robust regression slopes of relative rate of conversion to open water versus relative sea-level change rate across different rate intervals. Results are shown for four relative sea-level change rate intervals: Full range, <0, 0–θ, and >θ: (a) all tidal wetlands, (b) salt marshes, and (c) mangroves. θ denotes the rate threshold, identified as 8 mm yr^{-1} here. In each violin body, the thick and thin vertical black lines represent the 66% and 90% uncertainty ranges, respectively; the white dot represents the mean, and the black horizontal line represents the median. Each colored scatter point represents the result of a single Monte Carlo simulation. The inset provides an enlarged view of the Full-range, < 0 and 0–θ intervals. Purple values indicates the median slope value of each group. Grid cell counts and pairwise comparison probabilities for each interval are reported in Supplementary Table 1.



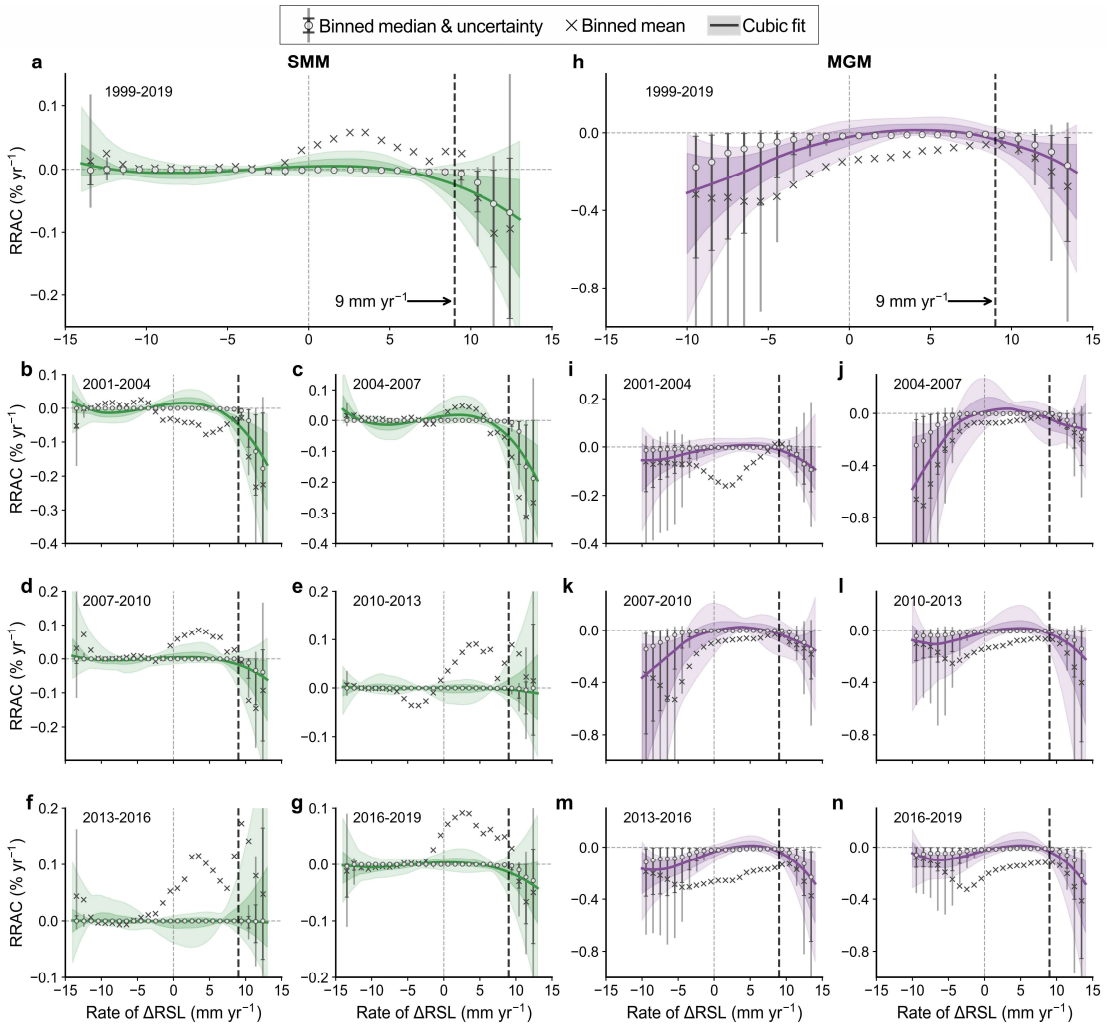
Supplementary Figure 4 | Effect of relative sea-level change on compensation of inundation-related losses by gains. Compensation is defined as gross gain minus loss to open water (i.e., inundation-related loss). Proportions of area change classified as loss, stable or gain per millimeter of relative sea-level change are shown for (a) all tidal wetlands, (b) salt marshes, and (c) mangroves. Numbers above bars indicate cell counts in each bin. The horizontal blue dashed line marks the 50% level. Darker and lighter error bars denote the uncertainty range of 66% (*likely range*) and 90% (*very likely range*), respectively. Relative rate of area change as a function of relative sea-level change rate are shown for (d) all tidal wetlands, (e) salt marshes and (f) mangroves. Circles and crosses denote the medians of binned medians and binned means, respectively. The grey error bars represent the 66% and 90% uncertainty ranges of binned medians. The colored curves show cubic fits to the binned medians, with darker and lighter shaded envelopes indicating the 66% and 90% uncertainty ranges. Calculations are based on 0.25° grid cells, including only cells with total wetland area > 1 km^2 and bins containing more than three grid cells.



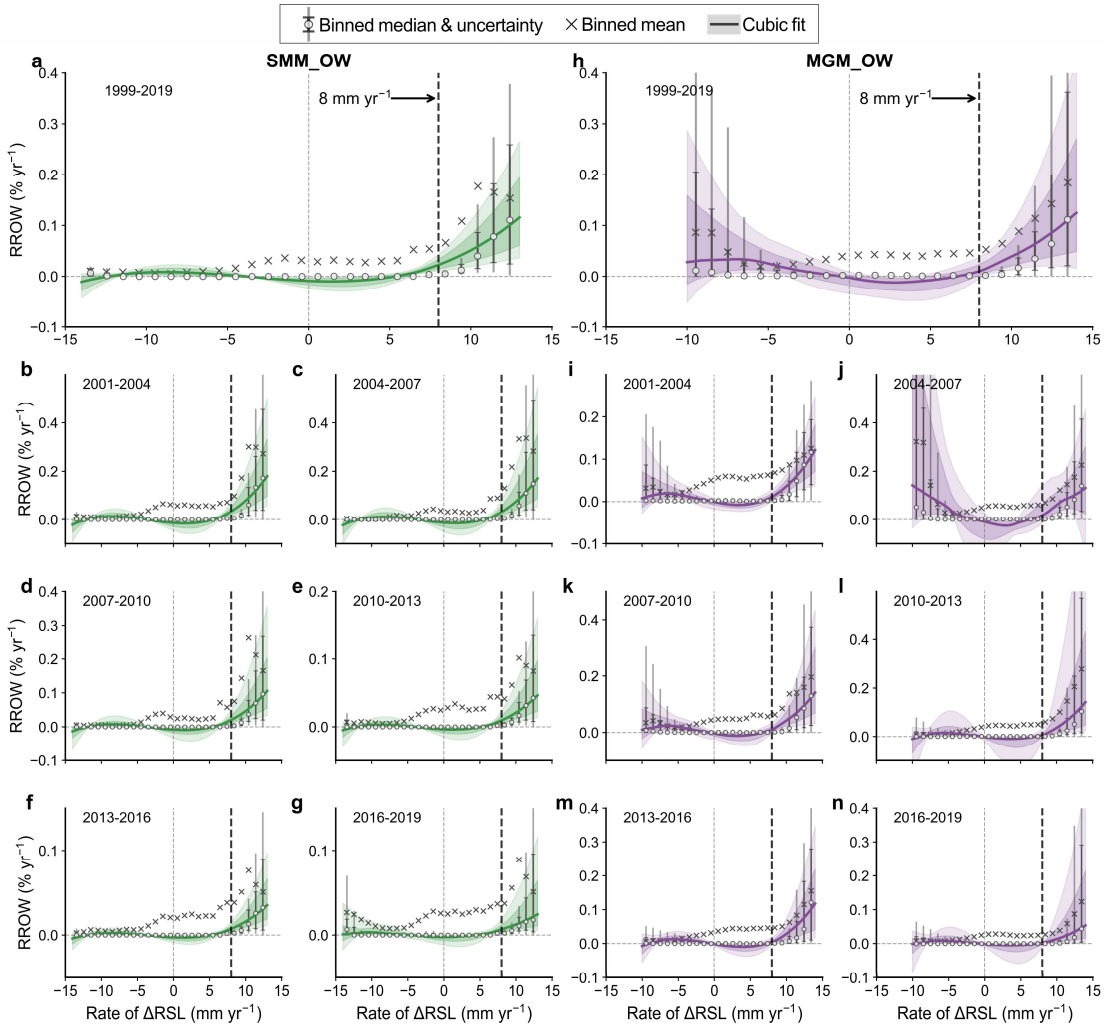
Supplementary Figure 5 | Examples of salt marshes under different relative change rate regimes along the nonlinear response curve. White dashed outlines denote the 0.25° grid cells used in the analysis. Shown are examples under (a) relative sea-level fall, (b, c) low-to-moderate relative sea-level rise, and (d) high relative sea-level rise.



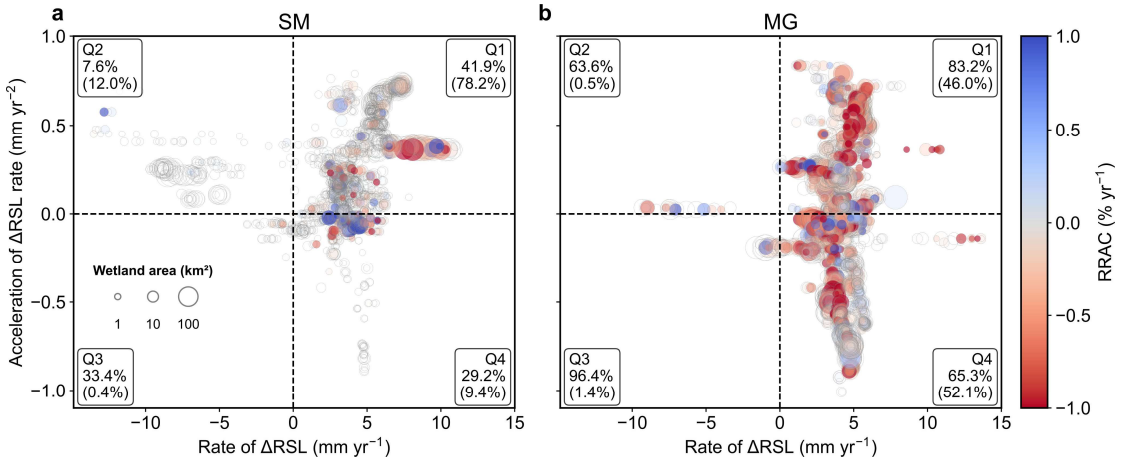
Supplementary Figure 6 | Examples of mangroves under different relative change rate regimes along the nonlinear response curve. White dashed outlines denote the 0.25° grid cells used in the analysis. Shown are examples under (a) relative sea-level fall, (b, c) low-to-moderate relative sea-level rise, and (d) high relative sea-level rise.



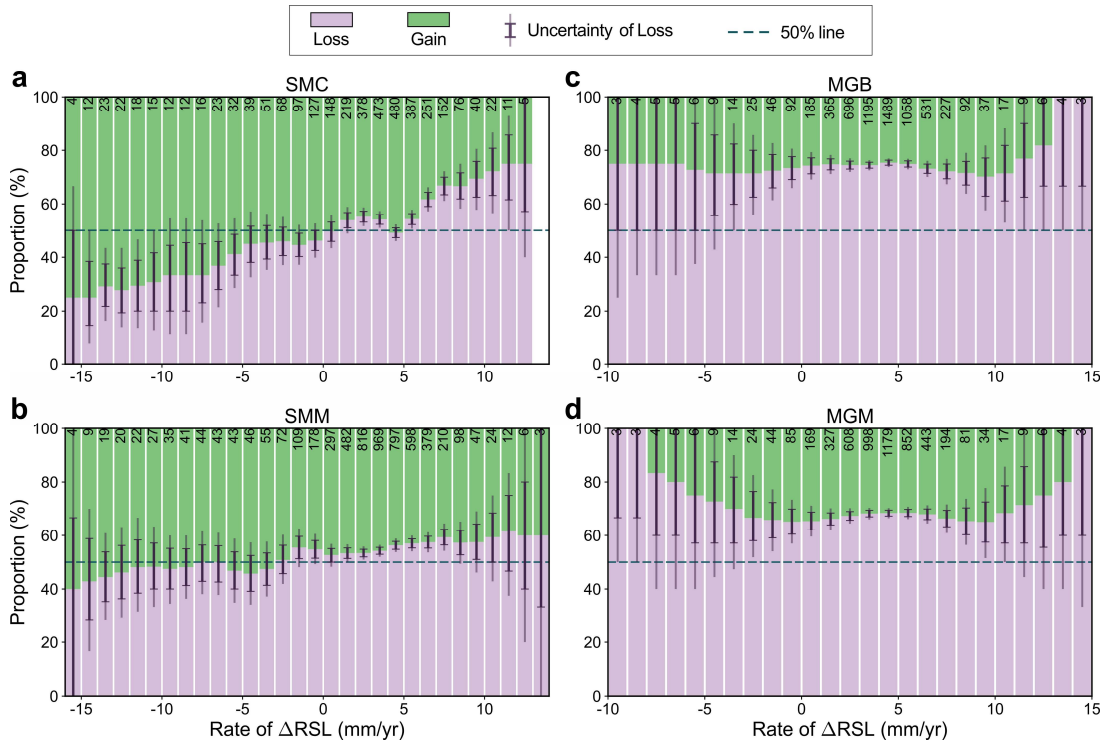
Supplementary Figure 7 | Comparison of net area change trends against relative sea-level change calculated over 20-year and 3-year intervals. Panels (a) and (h) show trends for salt marshes and mangroves, respectively, across the entire 1999–2019 period from the Murray et al. (ref. [7]) dataset. The panels below present trends for net change rate calculated in the same manner over successive 3-year intervals, with (b–g) corresponding to salt marshes and (i–n) to mangroves. The time span of the data used is indicated in the upper-left corner of each panel. Circles and crosses denote the medians of binned medians and binned means, respectively. Grey error bars represent the 66% and 90% uncertainty ranges. The black vertical dashed line marks the threshold position. Colored curves show cubic fits to the binned medians, with darker and lighter shaded envelopes indicating the 66% and 90% uncertainty ranges, respectively.



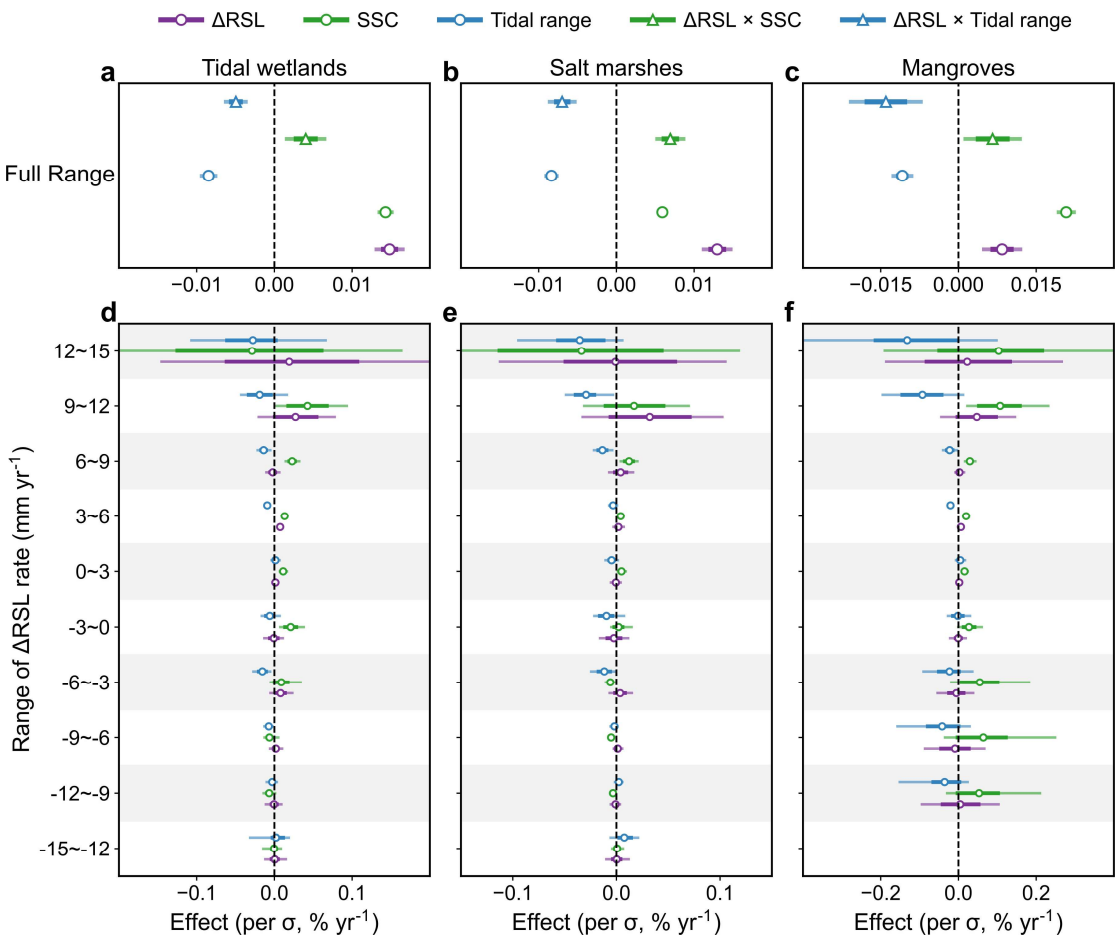
Supplementary Figure 8 | Comparison of inundation-related loss against relative sea-level change calculated over 20-year and 3-year intervals. Panels (a) and (h) show trends for salt marshes and mangroves, respectively, across the entire 1999–2019 period from the Murray et al. (ref. [7]) dataset. The panels below present trends for net change rate calculated in the same manner over successive 3-year intervals, with (b–g) corresponding to salt marshes and (i–n) to mangroves. The time span of the data used is indicated in the upper-left corner of each panel. Circles and crosses denote the medians of binned medians and binned means, respectively. Grey error bars represent the 66% and 90% uncertainty ranges. The black vertical dashed line marks the threshold position. Colored curves show cubic fits to the binned medians, with darker and lighter shaded envelopes indicating the 66% and 90% uncertainty ranges, respectively.



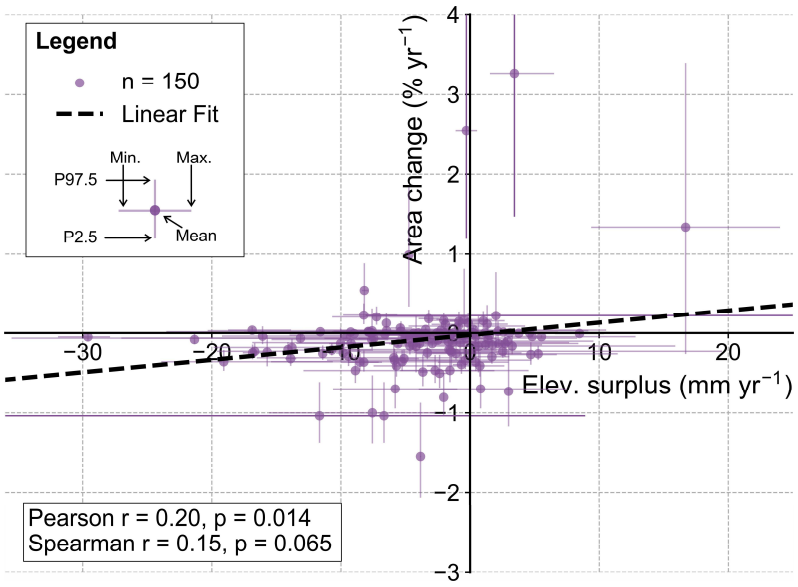
Supplementary Figure 9 | Wetland area change in the relative sea-level change rate-acceleration space. Panels (a) and (b) show the patterns for salt marshes and mangroves, respectively. Each circle represents a grid cell; circle size is proportional to total wetland area, and color indicates area change magnitude (red: negative values, blue: positive). The four quadrants are delineated by dashed lines at zero relative sea-level rate and zero acceleration. Quadrant labels display two areal proportions. The upper value in each quadrant indicates the percentage of that quadrant's wetland area experiencing area loss (change rate < −0.01% yr^{-1}). The lower value (in parentheses) indicates that quadrant's contribution to global total wetland (all quadrants sum to 100%). Comparison of loss percentages across quadrants, particularly between the upper-right quadrant (Q1, positive rate and acceleration) and the lower-right quadrant (Q4, positive rate but deceleration), highlights the potential role of acceleration in modulating inundation risk under rising relative sea level. The sea-level acceleration data are derived from ref.[8].



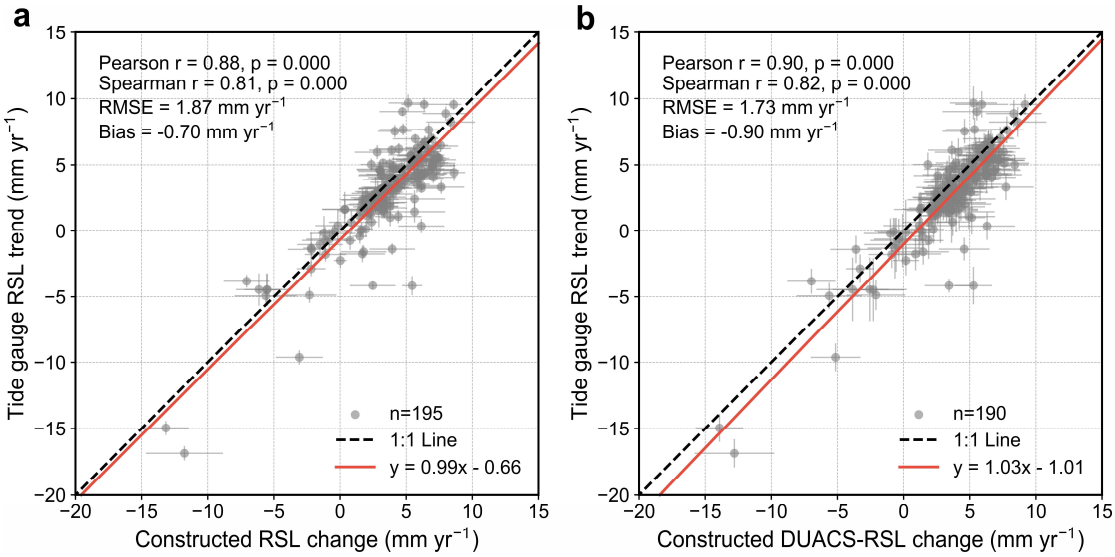
Supplementary Figure 10 | Gain-loss fractions across increasing relative sea-level change rate bins for individual datasets. Each panel corresponds to an individual wetland area change dataset: (a) salt marshes from Campbell et al. (ref.[9]); (b) salt marshes from Murray et al. (ref.[7]); (c) mangroves from Bunting et al. (ref.[11]); (d) mangroves from Murray et al. (ref.[7]). The blue solid line denotes the 50% proportion. Solid and dashed error bars indicate the 66% (*likely*) and 90% (*very likely*) uncertainty ranges, respectively. Only bins containing more than three grid cells are shown. These treatments seek to address the trade-off between global coverage and uncertainty: a single-dataset analysis minimizes uncertainty but limits global representativeness, whereas the combined analysis captures broader spatial patterns with higher uncertainty. Together, the two approaches provide complementary evidence that supports and cross-validates the main conclusions shown in Main text Fig. 2.



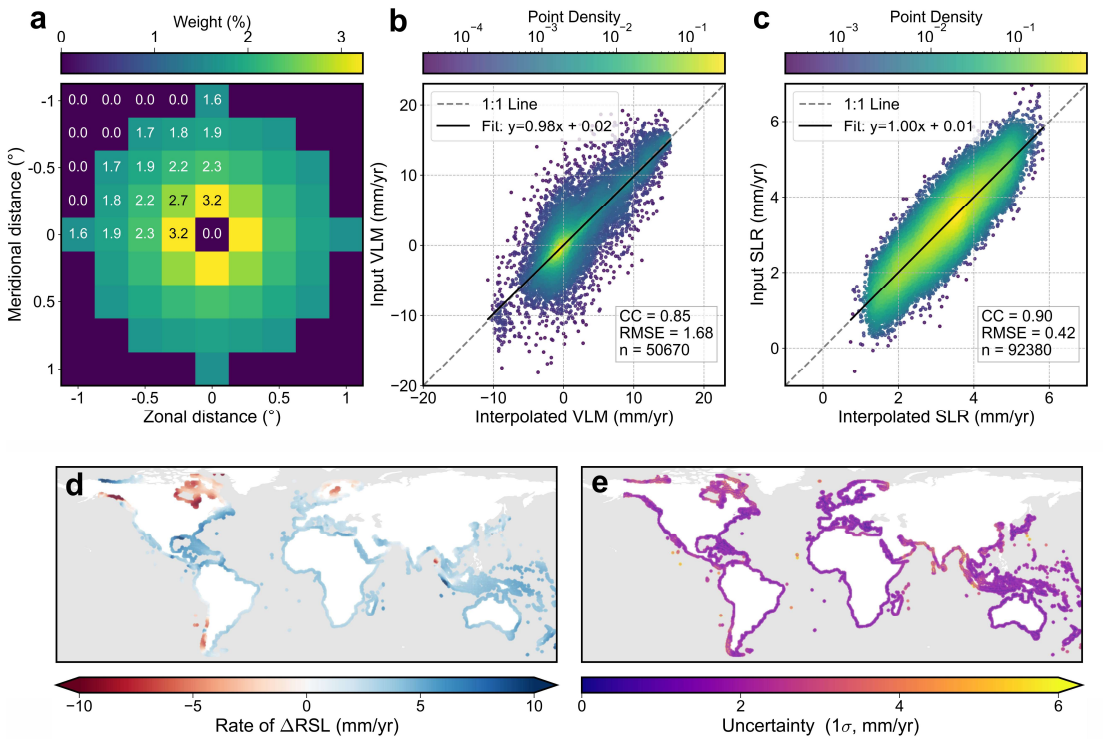
Supplementary Figure 11 | Effects of tidal range and sediment availability on inundation-related loss under relative sea-level change. Global multiple linear regressions incorporating interaction terms between relative sea-level change rate and each of tidal range and suspended sediment concentration, for (a) all tidal wetlands, (b) salt marshes, and (c) mangroves. Stratified multiple linear regressions excluding interaction terms, with effects estimated within 3 mm yr^{-1} intervals of relative sea-level rate for (d) all tidal wetlands, (e) salt marshes, and (f) mangroves. Circles denote mean coefficients of independent terms; triangles denote mean coefficients of interaction terms. Horizontal thick dark lines represent the 66% uncertainty range (aligned with the IPCC *likely range*), while thin, light lines represent the 90% uncertainty range (IPCC *very likely range*).



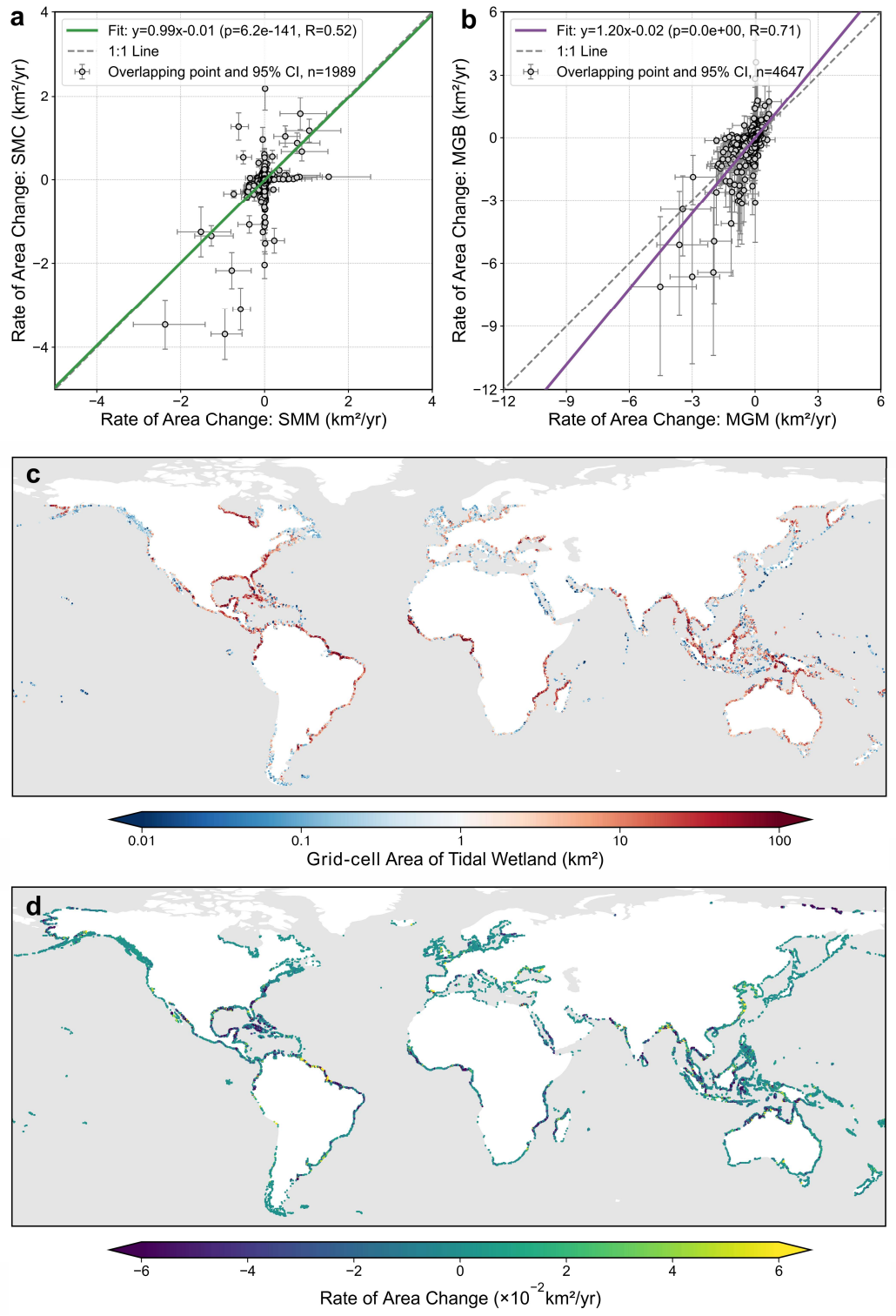
Supplementary Figure 12 | Comparison of grid-cell wetland area change with SET-MH records (n=150)**.** Relationship between grid-cell area change and measured elevation surplus/deficit. Cross symbols represent uncertainty ranges, with vertical bars showing the 2.5th–97.5th percentile range within each grid cell in this study, and horizontal bars indicating the minimum-maximum range of available in situ observations (refs. [3,11]) within the same grid cell. Most of SET-MH measurements span more than five years since the late 20th century. 702 valid points located in 150 grid cells were collected in this study.



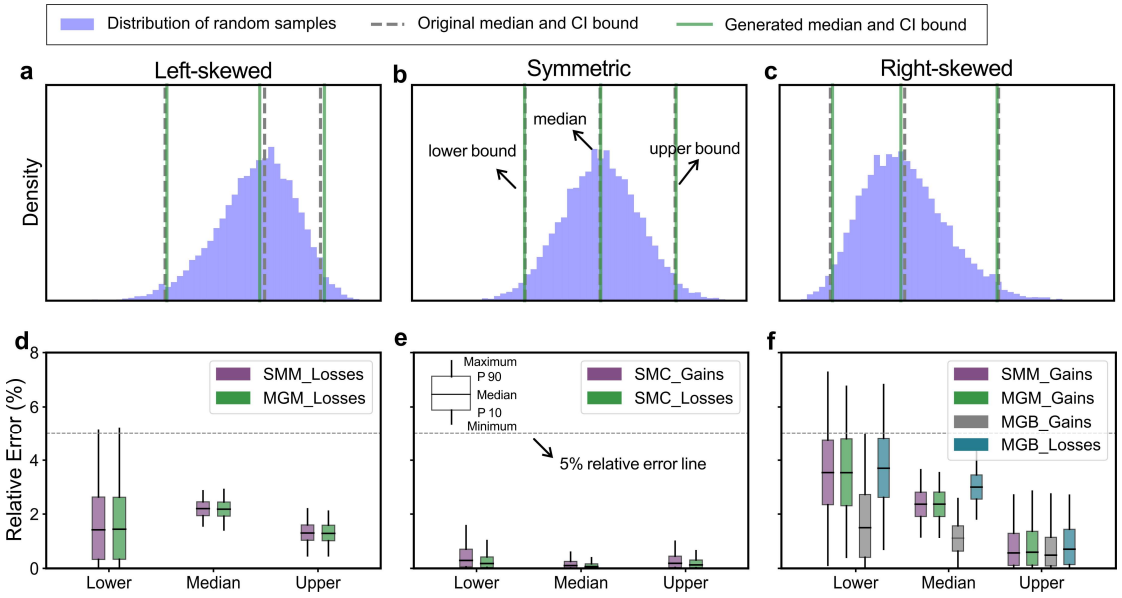
Supplementary Figure 13 | Comparison of grid-cell relative sea-level change rates versus tide gauge sea level trends. Absolute sea-level trends used to reconstruct relative sea-level change rates are based on (a) the downscaled trends of Prandi et al. (ref.[7]) and (b) the 0.125° sea surface heights from Copernicus Marine Service. Grey points represent valid paired observations where a tide gauge station falls within a wetland grid cell and provides record spanning ⩾20 years during 1993–2020. Tide gauge sea level trends are obtained from NOAA tide gauge network. Cross symbols indicate ±1σ uncertainty in both axes.



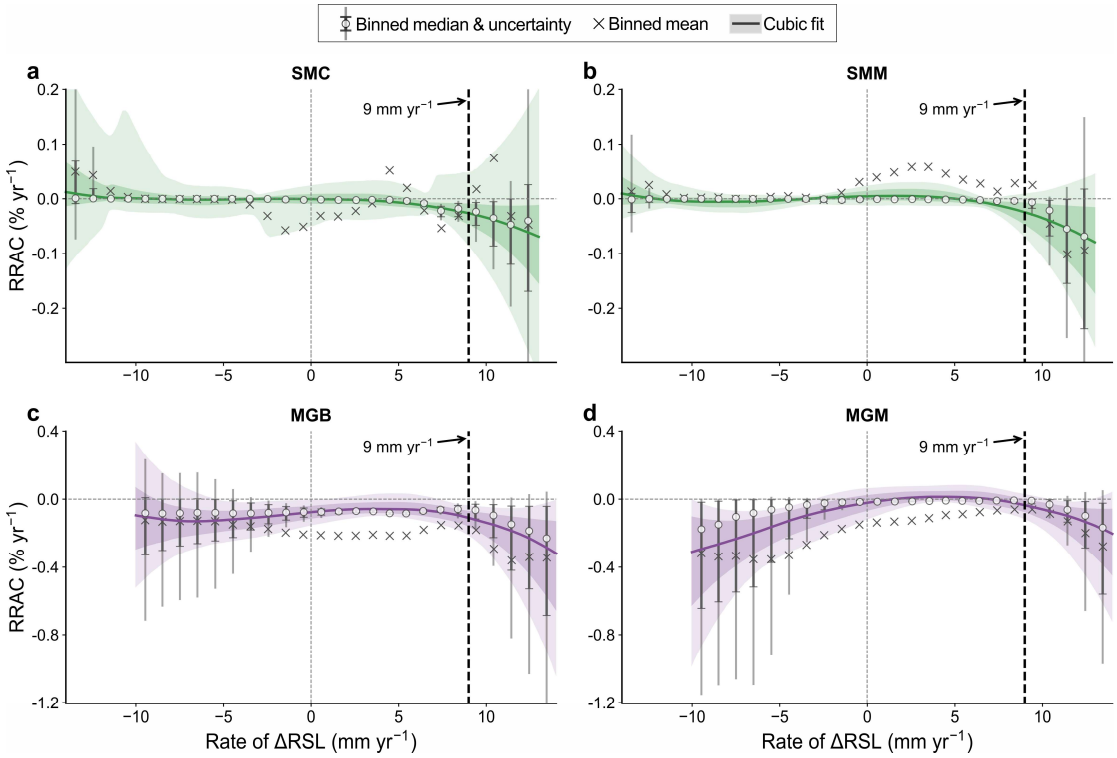
Supplementary Figure 14 | Quality control of the constructed relative sea-level change rate map. Panel (a) shows the inversed distance weight array used for convolution interpolation of vertical land motion and absoulute sea-level change grid cells. The center of the weight array is set to zero, making the interpolated values independent of the original values at the same grid cell. This allows accuracy assessment by comparing interpolated values with the original input data over tidal wetland zones, shown for (b) vertical land motion , and (c) absolute sea-level change. Panel (d) presents the final relative sea-level change rate map at 0.25° resolution, and panel (e) presentes the associated uncertainties at the 1σ level, derived from errors reported in the literature and propagated through the processing steps. Base map data are from Natural Earth in the public domain.



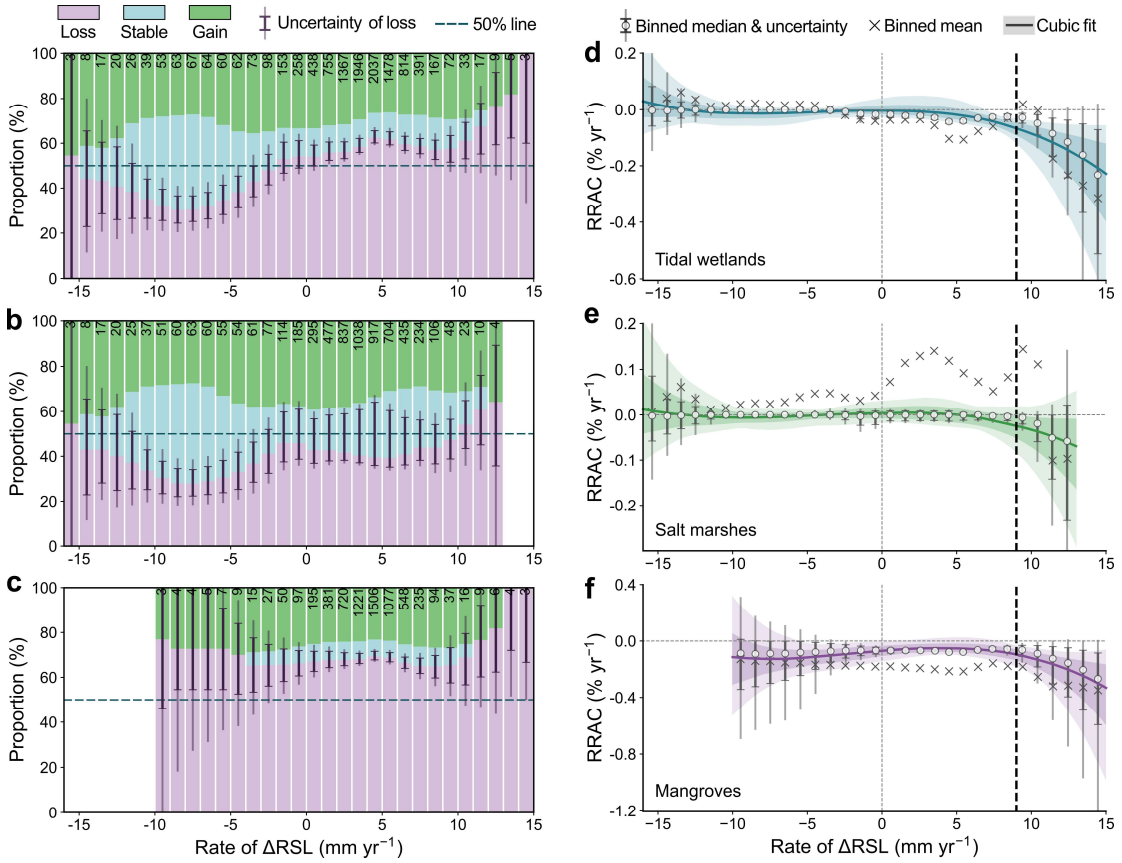
Supplementary Figure 15 | Cross-dataset comparison of salt marsh and mangrove area change rates at identical grid cells. Grid-level (0.25°) values and associated uncertainties of absolute area change rates are compared between the two datasets for (a) salt marshes and (b) mangroves. Linear fit and correlation coefficient are shown in each panel. Panel (c) shows the global map of tidal wetland extent, and panel (d) shows the global map of observed tidal wetland area change, combining both salt marshes and mangroves. Base map data are from Natural Earth in the public domain.



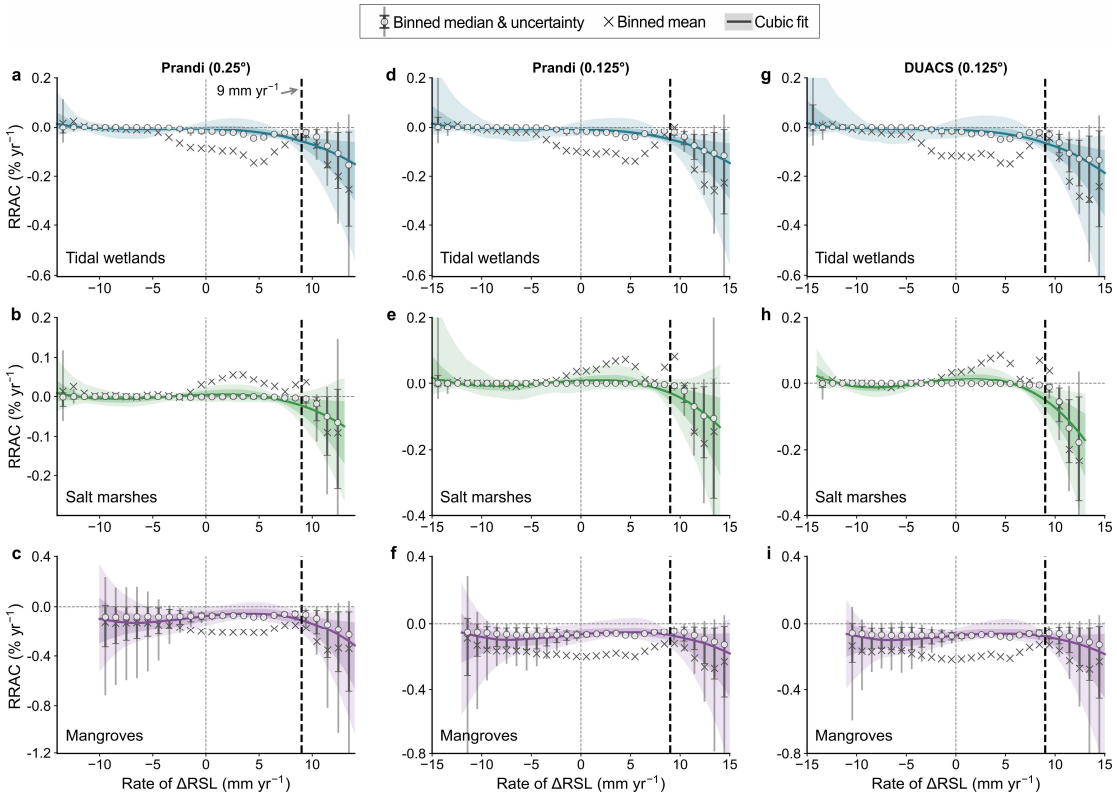
Supplementary Figure 16 | Errors estimation of the random sampling methods for tidal wetland area change under different given confidence interval skewness. Using reported error intervals with only three metrics (lower bound, median, upper bound), 10,000 iterations of random sampling were performed for gain and loss in each identified grid cell, with the sampling method adjusted based on the skewness of each dataset. Examples comparing reproduced and original metrics are shown for (a) left-skewed CI, (b) symmetric CI, and (c) right-skewed CI. Relative error was calculated as $RE = \frac{|x_R - x_o|}{x_o} \times 100\%$, where x_R and x_O are reproduced and original metrics for each grid cell. Panels (d–f) show the relative errors of the three metrics corresponding to the three skewness types across datasets. Overall, relative errors for all grid cells are below 8%, with more than 90% below 5% for all skewness types.



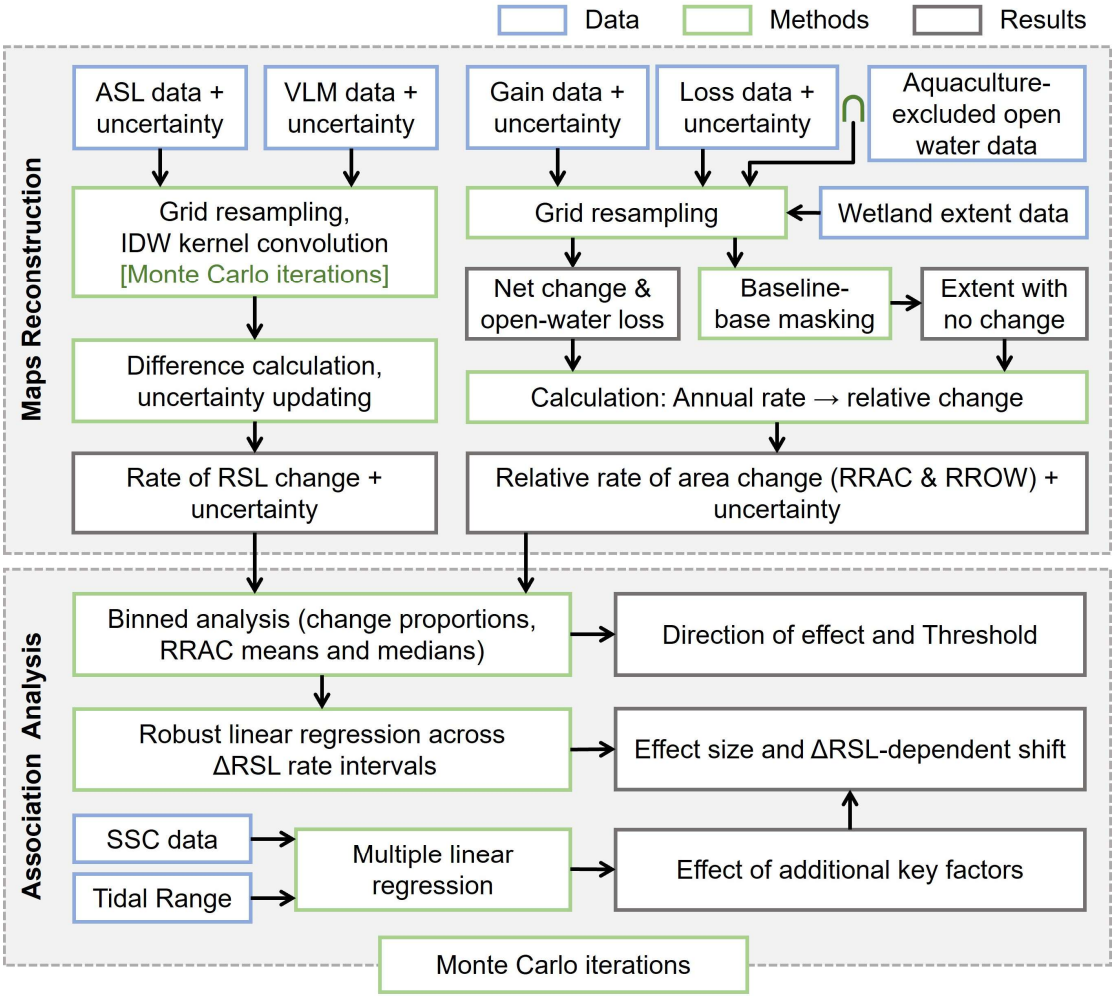
Supplementary Figure 17 | Trends of relative rate of area change across relative sea-level change rates from individual wetland area change datasets. Each panel corresponds to an individual wetland area change dataset: (a) salt marshes from Campbell et al. (ref.[9]); (b) salt marshes from Murray et al. (ref.[7]); (c) mangroves from Bunting et al. (ref.[11]); (d) mangroves from Murray et al. (ref.[7]). Circles and crosses denote the medians of binned medians and binned means, respectively. Grey error bars represent the 66% and 90% uncertainty ranges. The black vertical dashed line marks the threshold position. The colored curves show cubic fits to the binned medians, with darker and lighter shaded envelopes indicating the 66% and 90% uncertainty ranges, respectively.



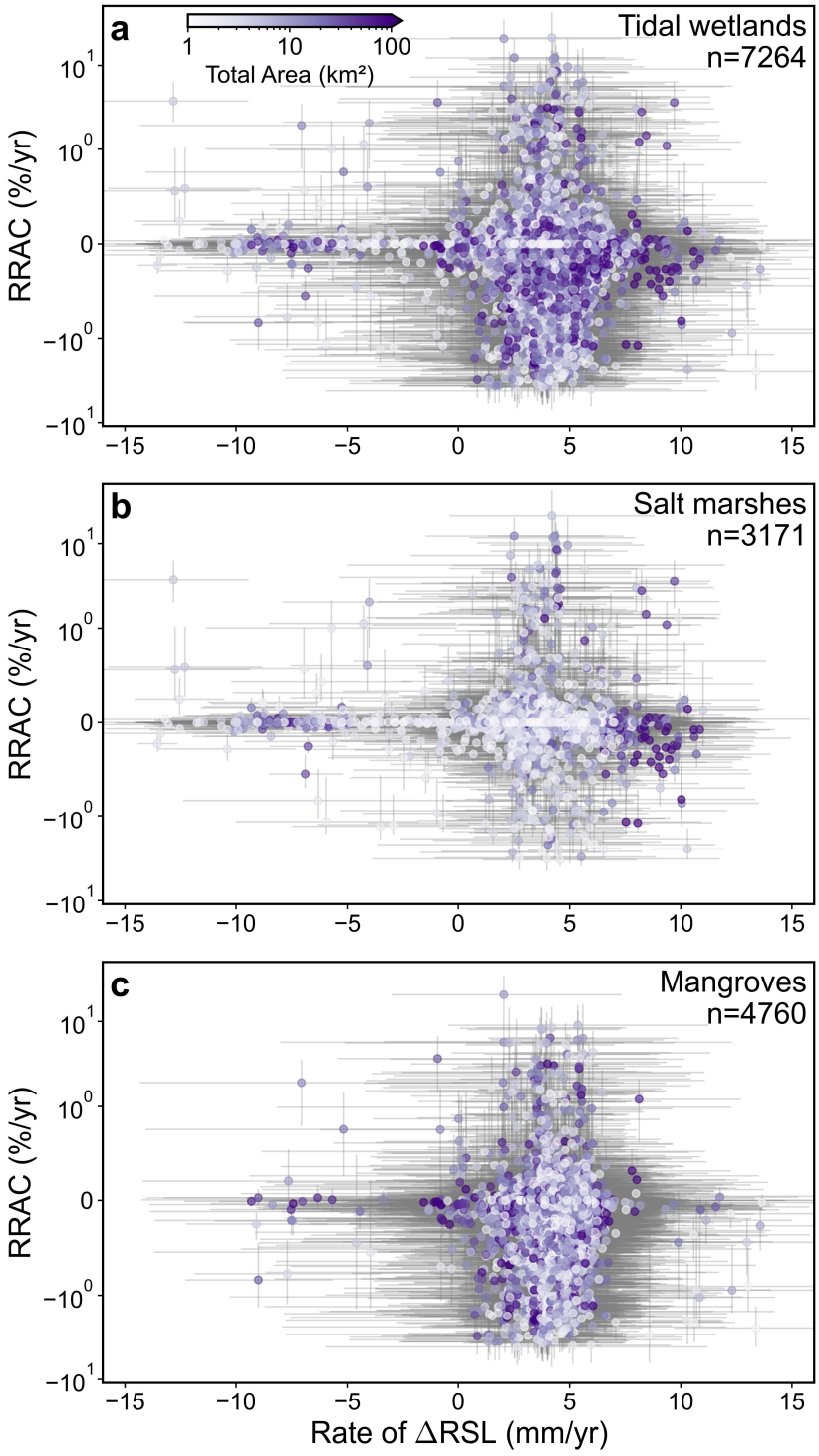
Supplementary Figure 18 | Effect of relative sea-level change on wetland surface area change. Proportions of area change classified as loss, stable or gain per millimeter of relative sea-level change are shown for (a) all tidal wetlands, (b) salt marshes, and (c) mangroves. Numbers above bars indicate cell counts in each bin. The horizontal blue dashed line marks the 50% level. Darker and lighter error bars denote the uncertainty range of 66% (*likely range*) and 90% (*very likely range*), respectively. Relative rate of net area change as a function of relative sea-level change rate are shown for (d) all tidal wetlands, (e) salt marshes and (f) mangroves. Circles and crosses denote the medians of binned medians and binned means, respectively. The grey error bars represent the 66% and 90% uncertainty ranges of binned medians. The black vertical dashed line marks the threshold position (see Supplementary Figure 1 for detailed identification). The colored curves show cubic fits to the binned medians, with darker and lighter shaded envelopes indicating the 66% and 90% uncertainty ranges. Calculations are based on 0.25° grid cells, including only cells with total wetland area > 0.1 km^2 and bins containing more than three grid cells.



Supplementary Figure 19 | Sensitivity of wetland area change to relative sea-level change across different grid-cell resolutions. Trends in area change magnitude as a function of relative sea-level change rate are shown for all tidal wetlands (a, d, g), salt marshes (b, e, h) and mangroves (c, f, i). The left column (a–c) shows results based on absolute sea-level trends from the 0.25° Prandi et al. (ref. [7]) product. the middle column (d–f) shows results based on the same Prandi et al. product, regridded to 0.125° resolution. the right column (g–i) shows results based on the native 0.125° sea surface height product from the Copernicus Marine Service. Circles and crosses denote the medians of binned medians and binned means, respectively. The grey error bars represent the 66% and 90% uncertainty ranges. The black vertical dashed line marks the threshold position. The colored curves show cubic fit to the binned medians, with darker and lighter shaded envelopes indicating the 66% and 90% uncertainty ranges. Analyses include only grid cells with total wetland area > 1 km^2 and bins containing more than three grid cells.

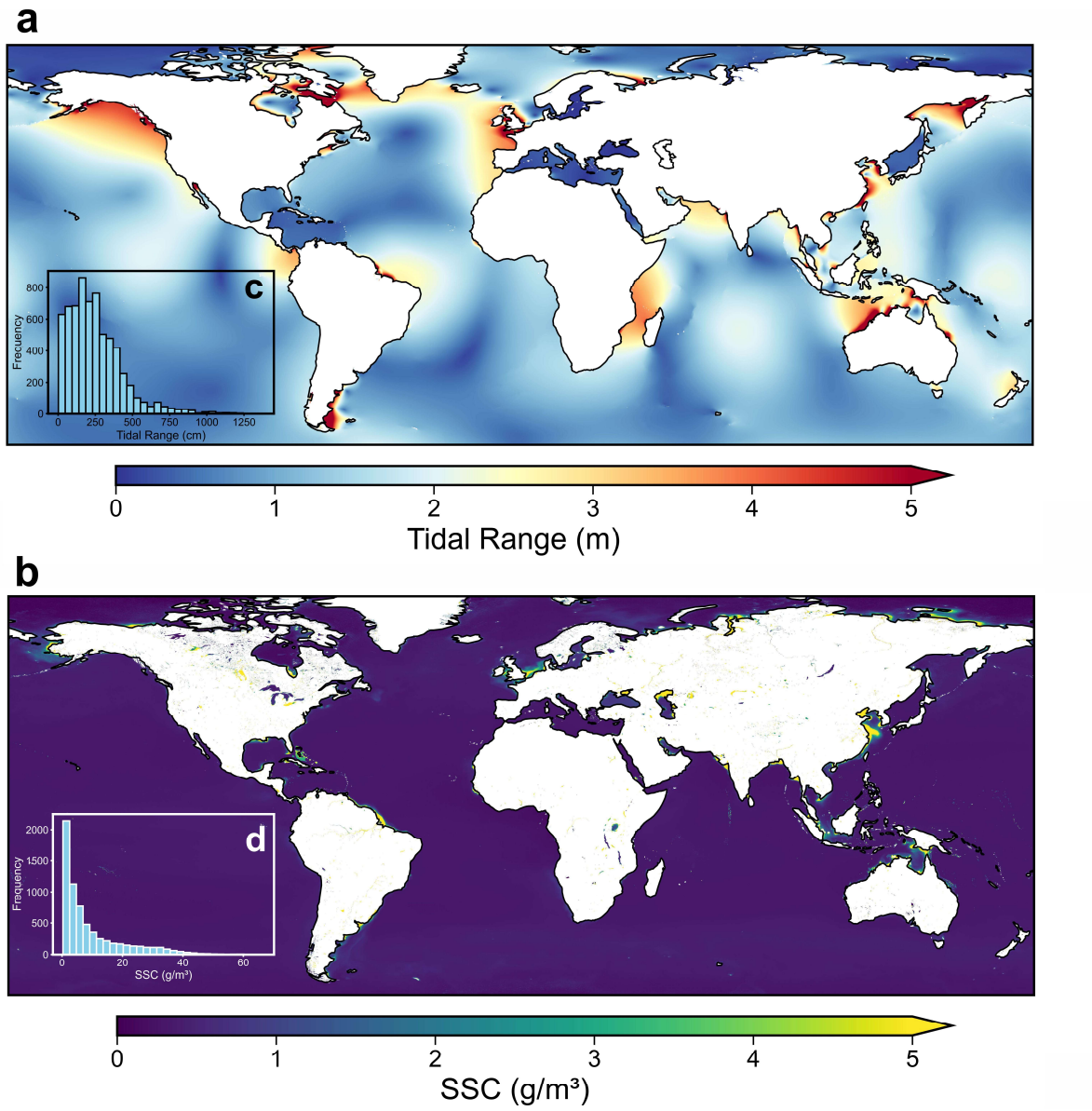


Supplementary Figure 20 | Workflow of data processing and analytical framework. The diagram summarizes the construction of relative sea-level change and wetland area change maps, including uncertainty propagation, as well as the subsequent association and attribution analyses (ASL: Absolute Sea-Level trend; VLM: Vertical Land Motion trend; RRAC: Relative Rate of net wetland Area Change; RROW: Relative Rate of conversion to Open Water). Blue boxes indicate data inputs, green boxes denote processing and analytical methods, and grey boxes represent derived results. The inverted U symbol represents the overlap (common grid cells) between datasets.



354

355 **Supplementary Figure 21 | Grid-cell observations with 95% uncertainty ranges.** Panels (a),
356 (b), and (c) show results for tidal wetlands, salt marshes, and mangroves, respectively. Error
357 bars indicate the 95% uncertainty ranges. Analyses include only grid cells with total wetland
358 area > 1 km^2.



Supplementary Figure 22 | Tidal range and suspended particulate material datasets used in the analysis. Panels (a) and (b) show global maps of tidal range and suspended sediment concentration, respectively. Panels (c) and (d) show the distributions of tidal range and suspended sediment concentration, respectively, for valid grid cells (i.e., those with available area-change and relative sea-level data and total wetland area > 1 km^2). Base map data are from Natural Earth in the public domain.

Supplementary Tables 1–5

Supplementary Table 1 | Count and area fraction of valid grid cells under different filtering criteria. Bold values represent the main analysis with 1 km² filtering.

Type	Filter		Count of grid cells	Gridded area (km²)	Fraction of total grid cell count (%)	Fraction of total wetland area (%)	Fraction of total area with valid ΔRSL (%)
Tidal wetlands	——		13652	2.05E+05	100.0	100.0	——
	+ ΔRSL valid		11837	1.92E+05	86.7	93.5	100.0
	+ Minimum gridded area (km²)	0.01	11564	1.92E+05	84.7	93.5	100.0
		0.10	10604	1.92E+05	77.7	93.5	100.0
		1.00	**7264**	**1.90E+05**	**53.2**	**92.7**	**99.2**
		10.00	3079	1.74E+05	22.6	84.6	90.5
		100.00	442	8.54E+04	3.2	41.6	44.5
Salt marshes	——		7787	5.29E+04	100.0	100.0	——
	+ ΔRSL valid		6606	4.33E+04	84.8	81.9	100.0
	+ Minimum gridded area (km²)	0.01	6544	4.33E+04	84.0	81.9	100.0
		0.10	6024	4.33E+04	77.4	81.8	99.9
		1.00	**3171**	**4.22E+04**	**40.7**	**79.7**	**97.3**
		10.00	851	3.43E+04	10.9	64.8	79.1
		100.00	80	1.18E+04	1.0	22.2	27.1
Mangroves	——		7803	1.52E+05	100.0	100.0	——
	+ ΔRSL valid		7120	1.49E+05	91.2	97.5	100.0
	+ Minimum gridded area (km²)	0.01	6868	1.49E+05	88.0	97.5	100.0
		0.10	6281	1.49E+05	80.5	97.5	100.0
		1.00	**4760**	**1.48E+05**	**61.0**	**97.1**	**99.5**
		10.00	2344	1.38E+05	30.0	90.6	92.9
		100.00	363	7.25E+04	4.7	47.6	48.8

Supplementary Table 2 | Slopes and their comparison probabilities from robust linear regressions (for RROW against ΔRSL rate). Values in parentheses indicate the *likely range*; values in square brackets indicate the *very likely range*.

(θ=8)	ΔRSL Interval (mm/yr)	Number of cells and proportion	Area proportion	Slope (×10^{-2} %/mm)	Probability of slopes comparison	
Tidal wetlands	Full	7264	——	0.10 (0.09,0.10) [0.09,0.11]	(Full) < (> θ)	99.9%
					(<0) < (> θ)	100.0%
	< 0	580 (8.0%)	7.2%	0.08 (0.07,0.10) [0.06,0.11]	(0 - θ) < (> θ)	100.0%
	0 - θ	6444 (88.7%)	88.0%	0.06 (0.04,0.07) [0.03,0.08]	(Full) < (0 - θ)	0.1%
					(<0) < (0 - θ)	11.7%
	> θ	240 (3.3%)	4.8%	1.05 (0.69,1.49) [0.48,1.85]	(Full) < (<0)	18.3%
Salt marshes	Full	3171	——	0.01 (0.01,0.01) [0.01,0.01]	(Full) < (> θ)	99.9%
					(<0) < (> θ)	99.9%
	< 0	420 (13.2%)	18.6%	0.00 (0.00,0.00) [0.00,0.01]	(0 - θ) < (> θ)	99.9%
	0 - θ	2610 (82.3%)	65.6%	0.00 (-0.00,0.01) [-0.01,0.01]	(Full) < (0 - θ)	0.3%
					(<0) < (0 - θ)	42.0%
	> θ	141 (4.4%)	15.8%	1.26 (0.71,2.02) [0.40,2.70]	(Full) < (<0)	0.5%
Mangroves	Full	4760	——	0.03 (0.01,0.05) [-0.00,0.06]	(Full) < (> θ)	99.8%
					(<0) < (> θ)	99.9%
	< 0	173 (3.6%)	4.0%	-0.06 (-0.15,0.02) [-0.23,0.07]	(0 - θ) < (> θ)	99.8%
	0 - θ	4460 (93.7%)	93.5%	0.03 (-0.00,0.05) [-0.02,0.07]	(Full) < (0 - θ)	46.6%
					(<0) < (0 - θ)	84.8%
	> θ	127 (2.7%)	2.5%	1.05 (0.60,1.63) [0.34,2.12]	(Full) < (<0)	14.0%

Supplementary Table 3 | Standard deviations of variables in multiple linear regressions by RSL change rate ranges (for grid cells with total wetland area > 1 km²).

	RSLC_interval	RSLC_std_mm_yr-1	SSC_std_g_m-3	TR_std_cm
Tidal wetlands	Full range	3.2	10.7	188
	3 mm yr-1 intervals	0.8	10.4	181
Salt marshes	Full range	4.1	11.4	217
	3 mm yr-1 intervals	0.8	10.3	190
Mangroves	Full range	2.2	10.3	166
	3 mm yr-1 intervals	0.8	9.9	122

Supplementary Table 4 | Probability of loss intensification in binned medians and means of RRAC′ across RSL change rate bins using different fitting methods (for grid cells with total wetland area > 1 km²). RRAC′: relative rate of area change calculated as gross gain minus loss into open water. For each wetland type, the upper and lower rows show fits to binned medians and binned means, respectively.

RRAC′ (Gain minus OW)	Probability of a declining linear trend	Probability of tail decay in Cubic fits
Tidal wetlands	31.9%	76.4%
	32.8%	87.6%
Salt marshes	63.2%	60.8%
	21.6%	83.6%
Mangroves	82.9%	40.7%
	84.1%	45.7%

Supplementary Table 5 | 95% uncertainty intervals of area change across datasets.

Dataset	Gross Loss (km²)	Lower CI bound for loss (km²)	Upper CI bound for loss (km²)	Proportion of lower CI bound for loss	Proportion of upper CI bound for loss	Gross gain (km²)	Lower CI bound for gain (km²)	Upper CI bound for gain (km²)	Proportion of lower CI bound for gain	Proportion of upper CI bound for gain
SMC (2000-2019)	**2733**	**2378**	**3088**	**0.15***	**0.15**	**1280**	**1025**	**1535**	**0.24**	**0.24**
SMM (1999-2019)	**1064**	**636**	**1306**	**0.4**	**0.23**	**1164**	**594**	**1884**	**0.49**	**0.62**
MGM (1999-2019)	**5561**	**3326**	**6827**	**0.4**	**0.23**	**1828**	**932**	**2960**	**0.49**	**0.62**
SMB (1996-2019)	**9348**	**5568**	**15825**	**0.4**	**0.69**	**4103**	**2238**	**7012**	**0.45**	**0.71**

*Note: Uncertainty reported in this study is originally expressed at the 90% confidence level. For consistency with other datasets, it is rescaled to the 95% confidence level assuming a normal distribution.

References

1. Törnqvist, T. E., Jankowski, K. L., Li, Y.-X. & González, J. L. Tipping points of Mississippi Delta marshes due to accelerated sea-level rise. Sci. Adv. 6, eaaz5512 (2020).
2. Saintilan, N. et al. Constraints on the adjustment of tidal marshes to accelerating sea level rise. Science 377, 523–527 (2022).
3. Saintilan, N. et al. Widespread retreat of coastal habitat is likely at warming levels above 1.5 °C. Nature 621, 112–119 (2023).
4. Horton, B. P. et al. Predicting marsh vulnerability to sea-level rise using Holocene relative sea-level data. Nat. Commun. 9, 2687 (2018).
5. Schuerch, M. et al. Future response of global coastal wetlands to sea-level rise. Nature 561, 231–234 (2018).
6. Kirwan, M. L. & Gedan, K. B. Sea-level driven land conversion and the formation of ghost forests. Nat. Clim. Change 9, 450–457 (2019).
7. Murray, N. J. et al. High-resolution mapping of losses and gains of Earth's tidal wetlands. Science 376, 744–749 (2022).
8. Prandi, P. et al. Local sea level trends, accelerations and uncertainties over 1993–2019. Sci. Data 8, 1 (2021).
9. Campbell, A. D., Fatoyinbo, L., Goldberg, L. & Lagomasino, D. Global hotspots of salt marsh change and carbon emissions. Nature 612, 701–706 (2022).
10. Bunting, P. et al. Global mangrove extent change 1996–2020: Global Mangrove Watch Version 3.0. Remote Sens. 14, 3657 (2022).
11. Jankowski, K. L., Törnqvist, T. E. & Fernandes, A. M. Vulnerability of Louisiana's coastal wetlands to present-day rates of relative sea-level rise. Nat. Commun. 8, 14792 (2017).